Bioorganic Chemistry 145 (2024) 107258

Contents lists available at ScienceDirect

Bioorganic Chemistry

journal homepage: www.elsevier.com/locate/bioorg

Design, synthesis, biological evaluation and docking study of some new aryl and heteroaryl thiomannosides as FimH antagonists

Anber F. Mohammed [a], Shimaa A. Othman [a], Ola F. Abou-Ghadir [a], Ahmed A. Kotb [b], Yaser A. Mostafa [a,1], Mohamed A. El-Mokhtar [c], Hajjaj H.M. Abdu-Allah [a,*]

[a] Pharmaceutical Organic Chemistry Department, Faculty of Pharmacy, Assiut University, Assiut 71526, Egypt
[b] Department of Microbiology and Immunology, Faculty of Pharmacy, Assiut University, Assiut, 71526, Egypt
[c] Department of Medical Microbiology and Immunology, Faculty of Medicine, Assiut University, Assiut 71515, Egypt

ARTICLE INFO

Keywords:
E. coli
Antiadhesion
FimH
Antagonist
Thiomannoside
Oxadiazole

ABSTRACT

FimH is a mannose-recognizing lectin that is expressed by *Escherichia coli* guiding its ability to adhere and infect cells. It is involved in pathogenesis of urinary tract infections and Chron's disease. Several X-ray structure-guided ligand design studies were extensively utilized in the discovery and optimization of small molecule aryl mannoside FimH antagonists. These antagonists retain key specific interactions of the mannose scaffolds with the FimH carbohydrate recognition domains. Thiomannosides are attractive and stable scaffolds, and this work reports the synthesis of some of their new aryl and heteroaryl derivatives as FimH antagonists. FimH-competitive binding assays as well as biofilm inhibition of the new compounds (**24**–**32**) were determined in comparison with the reference *n*-heptyl α-D-mannopyranoside (**HM**). The affinity among these compounds was found to be governed by the structure of the aryl and heteroarylf aglycones. Two compounds **31** and **32** revealed higher activity than **HM**. Molecular docking and total hydrophobic to topological polar surface area ratio calculations attributed to explain the obtained biological results. Finally, the SAR study suggested that introducing an aryl or heteroaryl aglycone of sufficient hydrophobicity and of proper orientation within the tyrosine binding site considerably enhance binding affinity. The potent and synthetically feasible FimH antagonists described herein hold potential as leads for the development of sensors for detection of *E. coli* and treatment of its diseases.

1. Introduction

Bacterial infectious diseases pose a major threat to human health worldwide and are greatly exacerbated when microorganisms grow as biofilms [1]. Biofilms enable the bacteria residing within them to resist the action of the human immune system and antibiotics [2]. The threat of biofilm-related infections has been greatly aggravated with the emergence of multidrug resistant bacteria [3]. Therefore, innovative therapeutic strategies are being developed to face these problems [3]. Among the therapeutic alternatives developed, the anti-adhesive strategy is of interest [3,4]. The concept is to disrupt the lectin-mediated adhesion of the pathogen to eukaryotic cells. This therapeutic approach should be less prone to bacterial resistance as the pathogens are not killed directly. As direct killing of bacteria by bactericidal agents leaves resistant strains alive and introduces evolutionary pressure, while anti-adhesion does not induce a selection pressure. On the other hand, any structural change in the adhesion properties of FimH by mutations would directly affect the pathogen's ability to bind to the host receptor thereby diminishing its virulence. This is why bacterial resistance due to anti-adhesion is not likely to occur. Several relevant bacterial targets have been identified, including the mannose-binding lectin FimH, displayed at the tip of long proteinaceous *Escherichia coli* (*E. coli*) organelles called pili [5,6]. *E. coli* is one of the predominant facultative anaerobes in the human GIT. Many strains of E. coli are non-pathogenic. However, there are small groups of E. coli that have evolved and developed pathogenic strategies that can cause several diseases such as diarrheal disease, Crohn's disease (CD) and serious sequelae, in the human host and are more commonly referred to as pathogenic E. coli [5,6]. There is other extraintestinal pathogenic *E. coli that* can cause a variety of infections in both humans and animals including urinary tract infections (UTIs), meningitis, and septicemia [6]. The adhesions of various pathogenic *E. coli* strains to host cells are primarily mediated through FimH

* Corresponding author.
E-mail address: hajjaj@aun.edu.eg (H.H.M. Abdu-Allah).
[1] Current address: Pharmaceutical Chemistry Department, Faculty of Pharmacy, Badr University in Assiut, Assiut 71511, Egypt.

https://doi.org/10.1016/j.bioorg.2024.107258
Received 29 January 2024; Received in revised form 29 February 2024; Accepted 1 March 2024
Available online 2 March 2024

which bind to mannosylated glycoproteins [7,8]. Therefore, FimH is a virulence factor, mannose-recognizing lectin expressed by *E. coli,* involved in bacterial biofilm formation and pathogenesis of UTIs and CD) [7,8]. The concept of blocking *E. coli* adhesion with FimH antagonists is classified as a promising and validated therapeutic target for UTIs and CD [9,10]. Extensive research efforts, based on structure-guided design and lead optimization, have led to a diverse set of small-molecule mannoside FimH antagonists with drug-like properties [11–16]. Some of these compounds are under clinical trials for CD and UTIs [12,13,16]. X-ray crystallographic data of mannosides binding to the FimH lectin domain revealed an extensive network of hydrogen bonds within the carbohydrate recognition domain (CRD) formed by Asn46, Asp47, Asp54, Gln133, Asn135, Asn138 and Asp140 [17,18]. In this complex, every hydroxy group of mannose establishes hydrogen bonding, resulting in high affinity and specificity [17,18]. Replacement of the α-D-mannose scaffold by different hexoses or sugars leads to a significant loss of affinity [18]. The binding affinity of FimH antagonist is largely affected by the ability of the aglycone to orient properly toward hydrophobic rim comprised of Phe1, Ile13 as well as the so-called 'tyrosine gate' of Tyr48, Ile52 and Tyr137 surrounding the entry to the deep, hydrophilic CRD [18]. Thus, the development of FimH antagonists mainly focused on the introduction of aglycones to mannose to improve binding by hydrophobic interactions. The flexibility of the tyrosine gate is due to the dynamic ability of Tyr48 to rotate between three positions. Importantly, the amino acids of the CRD of FimH are highly conserved among different *E. coli* isolates and many further Enterobacteriaceae, suggesting a reduced risk of resistance development and the affinity for mannosides is independent of *E. coli* pathotypes [18]. Based on these valuable findings, several monovalent mannose-based FimH antagonists were synthesized with diverse aglycones such as *n*-heptyl [19], biphenyl and its derivatives [20–25], thiazolylamino [26–28], indolinylphenyl and (aza)indolylphenyl [29], triazolyl [30–32], *N*-aryl substituted 3-hydroxypyridine-4-ones [33], branched *C*-glycoside [31,34,35], thiomannosides with alkyl or aryl substituted pyridine or pyridine [36] and isoquinolone [37].

The selectivity for FimH is of crucial importance. For example, heptyl and biphenyl mannosides, showed a 100 000-fold higher affinity for FimH compared to the tested human mannose binding proteins. Confirming that the binding selectivity is not a problem in the development of monovalent FimH antagonists [38].

A general problem of *O*-mannosides is their low bioavailability due to the low stability of the *O*-glycosidic bond. Efforts to improve metabolic stability of the mannosides included replacement of the glycosidic *O*- by *C*-, *N*-, and *S*- [26–36,39]. On the other hand, thiazolylaminomannosides with heterocyclic aglycones were investigated against CD in the gut, and showed improved relative inhibitory potency and affinity compared to heptyl α-D-mannopranoside [26]. Blocking FimH with high avidity ligands not only has therapeutic applications for treatment of UIs and CD but also could be used to develop sensors for *E. Coli* detection in medicine and the environment [40]. Inspired by above mentioned studies and findings and in continuation of our interest in developing glycomimetics to modify lectin-glycan interactions [41], herein we report the synthesis of new aryl and heteroarylthiomannosides as potent and stable FimH antagonists. These targets could find applications as therapeutics for *E. coli* infectious diseases such as UTIs and CD and detection of *E. coli* contamination in foods and water resources. The new compounds have been tested as inhibitors of *E. coli* adhesion and biofilm growth.

2. Focus and strategy

Our goal for this work is to develop effective ligands for FimH that could find applications as therapeutics for the prevention and treatment

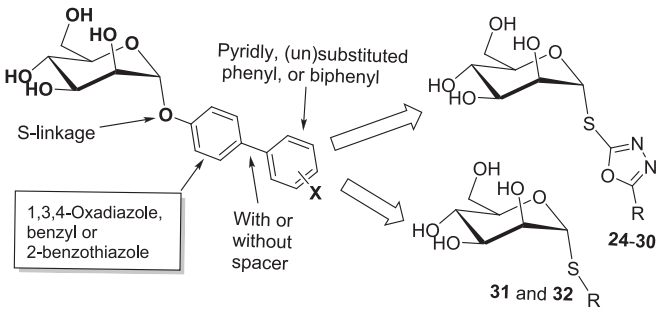

Fig. 1. Design of the new FimH antagonists.

of *E. coli* infections (UTI and CD) and as sensors for detection of *E. coli*. In our rational approach to design effective ligands, we carefully examined the reported studies and the CO-crystal structures of mannopyranosides with FimH [11–18]. Based on these studies and findings, the new aryl and heteroaryl thiomannosides were designed. Fig. 1 summarizes the proposed modifications to biphenyl-*O*-α-D-mannopyranoside. It is well-established that the mannose scaffold is essential for activity. Also, the nature of glycosidic linkage and the aglycone moiety play crucial role in determining the binding affinity to FimH and modifying their structures will influence the inhibitory potency, solubility, and stability.

Thioglycosides serve as more stable analogues of *O*-glycosides, since *S*-glycosidic bond is more resistant towards chemical and enzymatic hydrolysis [27,31,42]. Moreover, the replacement of glycosidic oxygen by sulfur results in greater affinity for the aromatic lined hydrophobic binding pockets [43]. Accordingly, thiomannoside is the main scaffold of the new FimH antagonists. On the other hand, biphenyl moieties have become a popular scaffold in many glycomimetics following the anticipation that the biphenyl motif is a replacement for a disaccharide (e. g. CD22 [44] and Sglec-4 [45]). The biphenyl residue has found a wide application in FimH glycomimetics, where it extends deeply in tyrosine gate, being engaged in π-stacking and hydrophobic interactions that increase binding affinity interactions within the binding pocket, thereby increasing potency [19]. Exploration of the substitution pattern and structural modifications on the biphenyl ring were extensively studied and afforded efficient FimH antagonists [20–25]. To date, the biphenyl mannosides are amongst the most promising antagonists for FimH with affinity in the low nanomolar range. However, their limited conformational flexibility and poor physicochemical properties; low solubility and stability, limit their suitability as oral treatment option [25]. Accordingly, it was decided to synthesize thiomannosides linked with aryl and heteroaryl moieties with diverse degree of size, polarity, and flexibility to modulate the FimH affinity, stability and solubility of the compounds. Particularly, Oxadiazoles, frequently occurring motifs in drug-like molecules and of known bactericidal activity against many bacteria including *E. Coli* [46–48]. *n*-heptyl α-D-mannopyranoside (**HM**) has also been synthesized and used as positive control. It remains one of the most potent FimH antagonists with an affinity in the low nanomolar range (K_D = 5 nM) [19]. The binding affinities of the new thiomannosides were determined in target and function-based assays.

3. Results and discussion

3.1. Chemistry

Scheme 1 depicts the synthesis of the target thiomannopyranosides (**24**–**32**). The starting 1,3,4-oxadiazole-2-thiols **(8**–**14)** were obtained by cyclization of the appropriate carbohydrazide (**1**–**7**) with CS_2 and KOH in ethanol. Among them (**8**–**11)** are reported [49–51], while (**12**–**14)** are new. Glycosylation of D-mannose pentaacetate with thiols (**8**–**14**) using

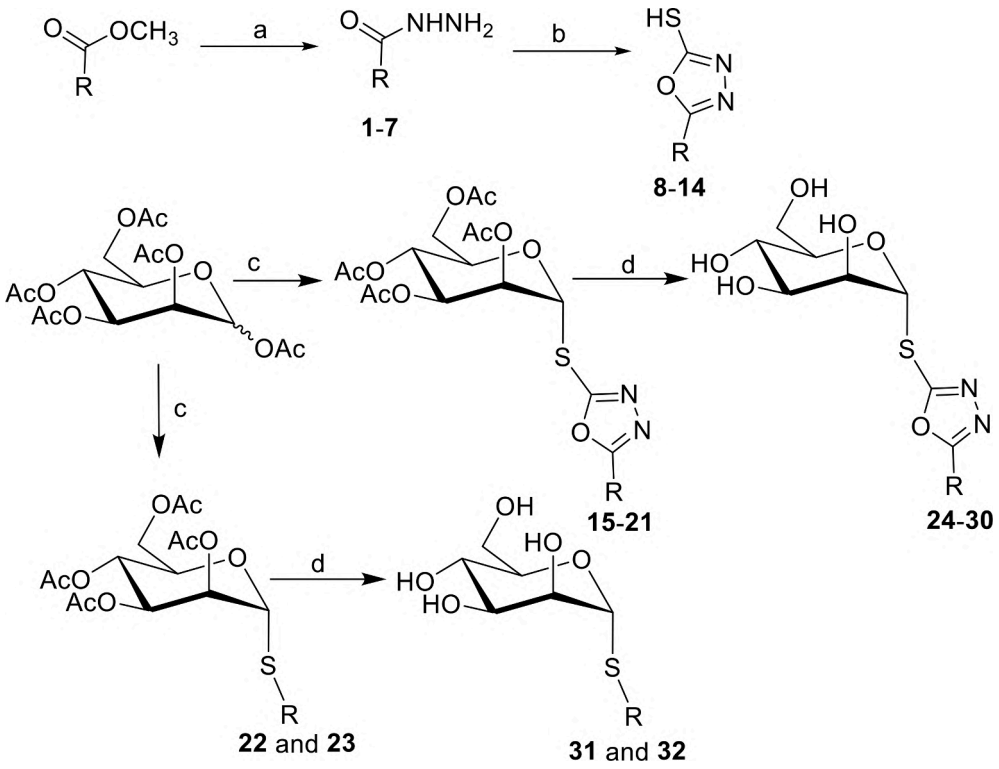

Scheme 1. Reagens and conditions: (a) NH_2NH_2, EtOH, reflux, 6 h; (b) CS_2, KOH, EtOH, reflux, 5 h, 70–85 % yield; (c) .**8**–**14**, benzylthiol or benzothiazole-2-thiol, $BF_3.Et_2O$, DCM 0 °C-rt, 24–48 h, 30–70 % yield; (d) (i) MeONa/MeOH, rt, 12–24 h (ii) H^+ exchange resin 70–90 % yield.

boron trifluoride etherate provided the acetylated aryl or heteroarylthio-α-D-mannopyranosides (**15**–**23**) in good yields (30—70 %). Neighboring group participation of the axial 2-acetyl results in exclusive formation of the α-anomer [31,36]. Subsequent deacetylation with sodium methoxide in methanol gave the target thiomannosides (**24**–**32**) in yields (70–90 %). The synthesis of benzylthio-α-D-mannopyranoside (**31**) is reported in a different procedure [52,53], while the reference compound; *n*-heptyl α-D-mannopyranoside was synthesized as reported [19,54]. All the new compounds were characterized by physical, spectral data and elemental analysis.

R	Hydrazide	Oxadiazole-2-thiol	Protected thiomannosides	Deprotected thiomannosides
Phenyl	**1**	**8**	**15**	**24**
4-Hydroxyphenyl	**2**	**9**	**16**	**25**
4-Pyridyl	**3**	**10**	**17**	**26**
3-Pyridyl	**4**	**11**	**18**	**27**
4-Bromobenzyl	**5**	**12**	**19**	**28**
4′-Hydroxybiphen-4-ylmethyl	**6**	**13**	**20**	**29**
Biphen-4-yloxymethyl	**7**	**14**	**21**	**30**
Benzyl	–	–	**22**	**31**
Benzothiazole-2-yl	–	–	**23**	**32**

3.2. Biology

3.2.1. In vitro binding and functional assays of FimH activity

Different *in vitro* assays have been utilized to measure both the binding affinity and the functional potency against FimH [12]. First, to screen for FimH activity, compounds were tested by enzyme-linked lectinosorbant assay (ELLSA). Then, the functional inhibition of FimH activity was tested using an epithelial cell-culture adherence model [55]. This assay measures the ability of the compounds to prevent or disrupt *E. Coli* adhesion to T24 urinary epithelial cells. T24 cells display the mannosylated receptor at their surface, which is overexpressed in patients with UTI and has been shown to play a key role in *E. Coli* adhesion to the bladder. Finaly, a biofilm inhibition assay to quantitatively measure a compound's ability to disrupt assembly of a bacterial biofilm was carried out [56,57].

3.2.1.1. Effect of the new thiomannosides on adhesion of E. coli to T24 urinary epithelial cells. By means of a cell-based assay, the new compounds were evaluated for their ability to inhibit the adhesion of clinical *E. coli* strain (isolated from patient with UTI) to T24 human urinary bladder epithelial cell. T24 cells express a mannosylated protein that mediate *E coli* adhesion to the cells. The residual % of bacterial adhesion obtained in the presence of test compounds at 0.5 μM concentration compared to control untreated cells, is presented in Table 1. The FimH antagonist, *n*-heptyl α-D-mannopyranoside (**HM**), with its nanomolar potency is commonly used as a posiive control [15,22,26,30] and it was used for the same purpose in this study. Most designed thiomannosides were shown to efficiently interfere with the binding of *E coli* to T24 cells with residual adhesion % ranging from 21.00 to 88.33. Three out of nine compounds tested were more effective than **HM**. Benzothiazol-2-yl derivative (**32**) was the most potent among the tested compound with a residual adhesion level of only 21.00 %±6.00 which was 2.7 folds lower than **HM's** residual adhesion (57.33 %±3.51). Also, benzyl thiomannoside (**31**) was found to markedly decrease the bacterial adhesion to almost comparable level of (**32**) (24.33 %±8.08). This highlights their competing binding forces and superior effects over oxadiazole counterparts. Amongst oxadiazole derivatives, (**29**) with 4 -hydroxybiphen-4-ylmethyl aglycone exhibited the greatest decrease of adhesion to 40.67 %±5.13. On the other hand, an average residual adhesion of 75.5 % was observed for (**28**) and (**30**) with 4-bromobenzyl and biphen-1-yloxymethyl aglycones, respectively. Also, oxadiazole mannosides (**24**–**27**) with phenyl, 4-hydroxyphenyl, 4-pyridyl and 3-pyridyl aglycones, respectively, almost disrupt the bacterial adhesion to 83.00–88.33 %. From these findings we could conclude that adding a

Table 1
Results of FimH-competitive binding assays (% Residual adhesion and % Antibody binding to FimH) as well as % biofilm inhibition of compounds **(24–32)** and **HM***.

Compd. No	R	%Residual adhesion	%Antibody binding to FimH	%Biofilm inhibition
24	Phenyl	83.00 ± 7.94	73.00 ± 14.73	34.72 ± 13.16
25	4-Hydroxyphenyl	84.67 ± 8.39	91.33 ± 10.02	13.26 ± 32.18
26	4-Pyridyl	88.33 ± 7.64	88.00 ± 11.00	13.57 ± 20.41
27	3-Pyridyl	84.33 ± 14.01	89.67 ± 9.50	0.28 ± 2.88
28	4-Bromobenzyl	75.00 ± 9.54	76.67 ± 6.03	32.70 ± 26.12
29	4'-hydroxybiphen-4-ylmethyl	40.67 ± 5.13	67.00 ± 8.18	82.87 ± 14.17
30	Biphen-1- yloxymethyl	76.00 ± 11.14	74.00 ± 9.16	20.33 ± 12.74
31	Benzyl	24.33 ± 8.08	41.00 ± 5.29	99.99 ± 0.11
32	Benzothiazole-2-yl	21.00 ± 6.00	16.67 ± 3.51	98.95 ± 0.27
Control	HM	57.33 ± 3.51	41.33 ± 5.51	57.00 ± 8.80
–	control untreated cells	97.67 ± 2.52	–	–
–	FimH	——	97.67 ± 2.52	–

* The activity of all antagonists was measured twice in duplicates. The antagonist **HM** was used as a reference compound and tested in parallel to ensure comparability.

methylene unit between oxadiazole moiety and the aryl chain improved activity of **28–30** over other oxadiazole analogues **24–28**. Moreover, linking the aryl chain to oxadiazole scaffold with more polar and flexible methyloxy chain remarkably declines the activity of **(30)** compared to **(29)**. That conclusion might propose the length and character of linker between biaryl aglycone suitable to maintain mannosylated activity.

3.2.1.2. Competitive enzyme-linked lectinosorbent assay (ELLSA). To determine the compounds' potency for prevention of FimH binding of *E. coli*, an enzyme-linked lectinosorbnt assay (ELLSA) was used. Briefly, RNaseB (Merck Millipore, Germany), a mannosylated glycoprotein, was coated on microplates and then incubated with FimH, with or without test compounds. The binding of FimH to RNaseB was detected by adding rabbit-anti-FimH antibodies followed by anti-rabbit Horseradish peroxidase (HRP)-labeled secondary antibody (Enzo Life Sciences, USA). Finally, 3,3′,5,5′-tetramethylbenzidine (TMB) was added, and the absorbance was read at 450 nm using a microplate reader (BioTek, USA). Most compounds achieved marked ability to inhibit oligomannose glycoepitopes as shown in Table 1. Analogous to residual adhesion outcomes, compounds **(29)**, **(31)** and **(32)** were found to be the most potent ones as FimH antagonist amongst test compounds. Benzothiazol-2-yl thiomannoside **(32)** was considerably more potent than **(HM)** and was the most potent one among tested compounds with FimH antibody binding inhibitory % 16.7 %±3.5. In addition, benzyl substituted derivative **(31)** competed markedly with FimH binding at an inhibitory % of 41.00 %±5.29 comparable to **HM**'s inhibitory one 41.33 %±5.51. Also, **(29)** with 4 -hydroxybiphen-4-ylmethyl aglycone was the most superior one over the rest of oxadiazole mannosides at an inhibitory % of 67.00 %±8.19. Inhibitory activities tend to increase with **(24)**, **(28)** and **(30)** at an average % of 74.5 for the reasons suggested above. Moreover, compounds **(25–27)** were not associated with significant reduction in binding affinities.

3.2.1.3. Effect on biofilm formation. In order to test the ability of the compounds to disrupt the biofilm formation, microtiter plate method was used to quantitatively estimate the biofilm formation in presence of the test compounds compared to control untreated wells. Bacterial biofilms are generally able to dispute current UTIs antibiotic remedies as well as enhance chance for recurrence and bacterial resistance. Results revealed that the three utmost potent FimH antagonists of the present study were also able to significantly inhibit the ability of bacteria to form biofilm. Compounds **(31)**, **(32)** and **(29)** exhibited excellent biofilm inhibitory % of 99.99 ± 0.11, 98.95 ± 0.26 and 82.87 ± 14.17, respectively compared to **HM** activity 57.00 %±8.79. Other test compounds showed lowest inhibitory activity ranging from 34.72 to 13.26 %.

3.2.2. Molecular docking

In silico docking simulations and molecular descriptor calculations were performed using Molecular Operating Environment (MOE) software [58]. All synthesized compounds (**24–32**) were docked at the active site of FimH lectin domain from *E. coli* K12 (PDB: 4XO8) [8] in order to investigate ligand binding mode and rationalize the biological results. The simulation results of the compounds were compared to the known co-crystallized ligands (**HM**) and NeoTazMan [28]. Data are shown in Table 2. Accuracy of docking protocol was validated by means of redocking the co-crystallized ligand into FimH binding site where *S* score obtained for docked ligand was −7.74 kcal/mol with RMSD value of 1.06 Å. Also, **HM** probes the space of the protein active site in a manner that maintains both the mannose moiety and the heptyl aglycone in a good geometry, Fig. 2. The active site was observed to comprise of a tight polar sugar binding pocket which is surrounded by hydrophobic ridge defined by tyrosine gate residues (Tyr48, Ile52 and Tyr137), support residues (Phe1, Ile13, and Phe142), in addition to Thr51 residue. Also, there is a salt bridge of Arg98–Glu50 adjacent to the tyrosine gate. Based on docking score analysis all designed compounds showed comparable scores (-6.36 to −8.23) to HM which indicate their FimH binding affinity. Inspection of ligand protein complexes revealed that all new thiomannosides conserve mannose binding pattern where the hydrophobic aglycones point out of the FimH-mannose binding site. The ligand α-$_D$ mannose moiety forms a network of multiple H-bond interactions with side chains of Asp54, Asn135, Asp140 and Gln133 as well as the backbone chains of Phe1 and Asp47 compared to **HM** and **NeoTazMan** (suppl. data). These conserved interactions approve the FimH binding affinity of designed compounds. In addition, ligand mannose hydroxyl group accepts water651-bridged H-bond with Gln133 side chain and Phe1 backbone in compounds **(25)**, **(26)** and **(27)**. Moreover, sulfur linker in compounds **(29)** and **(31)** accepts water782 mediated H-bond to Asn138 and Asp140 which augment their tight binding within sugar pocket. Later finding confirms that *S*-linked mannosides could be stabilized by retaining water-mediated H-bonds within the active site similarly to reported *O*- and *N*-mannosides (such as HM and NeoTazMan) [28]. Also, docking results revealed that most designed aryl aglycones resembled tazman thiazolyl moiety orientation [28] and exhibited proper orientation within tyrosine gate forming hydrophobic interactions as well as π-stacking with Tyr48 and Tyr137.

Table 2
Ligand-protein complex interactions of the tested compounds (**24**–**32)** within the active site of FimH with (PDB: 4XO8).

Compd.	Score kcal/mol	H-bond interactions (Å)	Hydrophobic interactions	Other interactions (Å)
HM	−7.74	Asp54 (2.56, 2.54) Asp140 (2.70) Phe1 (2.79, 2.85) Asp47 (2.91) Asn135 (2.85) Gln133 (3.03)	Tyr48, Tyr137, Ile13, Ile52, Asp140, Phe1	H_2O782 water bridge to Asp140 (2.86) H_2O651 water bridge to Ile13, Gly14, Gln133 (2.80)
24	−6.54	Asp54 (2.81) Asp54 (2.77) Asp140 (2.79) Asn135 (3.00) Phe1 (2.98) Asp47 (2.95)	Tyr48, Tyr137, Ile13, Ile52, Asp140, Phe1	———
25	−6.61	Asp54 (2.80) Asp54 (2.77) Asp140 (2.82) Asn135 (3.00) Phe1 (2.98) Asp47 (2.95)	Tyr48, Tyr137, Ile13, Ile52, Asp140, Phe1	———
	−6.36	Asp54 (2.66) Asp140 (2.85) Asn135 (2.88) Phe1 (2.89) Gln133 (2.96)	Tyr48, Ile13, Ile52, Phe1, Asp47	Tyr48 pi-H (3.73) H_2O651 water bridge to Ile13, Gly14, Gln133 (2.85)
26	−6.55	Asp54 (2.77, 2.81) Asp140 (2.79) Asn135 (3.00) Phe1 (2.98) Asp47 (2.95)	Tyr48, Tyr137, Ile13, Ile52, Asp140, Phe1	———
	−6.41	Asp54 (2.68) Asn46 (2.83) Asp140 (2.84) Asn135 (2.90) Phe1 (2.88) Gln133 (3.02)	Tyr48, Ile13, Ile52, Phe1, Asp47	H_2O651 water bridge to Ile13, Gly14, Gln133 (2.89)
27	−6.70	Asp54 (2.77, 2.81) Asp140 (2.79) Asn135 (3.00) Phe1 (2.98) Asp47 (2.95)	Tyr48, Ile13, Asp47, Ile52, Asp140	———
	−6.50	Asp54 (2.68) Asn46 (2.83) Asp140 (2.84) Asn135 (2.90) Phe1 (2.88) Gln133 (3.02)	Tyr48, Tyr137, Ile13, Ile52, Asp140, Phe1	H_2O651 water bridge to Ile13, Gly14, Gln133 (2.89)
28	−6.92	Asp54 (2.73, 2.76) Asp140 (2.93) Asn135 (2.92) Phe1 (2.91, 2.94) Asp47 (2.88) Asp140 (2.84) Gln134 (3.34)	Tyr48, Asp47, Ile13, Ile52, Phe1, Asp140	H_2O782 water bridge to Asp140 (3.32)
29	−6.77	Asp140 (3.03) Asp54 (3.35) Gln133 (3.32) Asn135 (3.10) Phe1 (2.88, 3.04) Asp47 (3.43)	Tyr48, Ile13, Ile52, Glu50, Arg98, Asp48, Asp140, Tyr137, Phe1	Tyr48 (pi-pi) (3.86) H_2O782 water bridge to Asp140 (3.21)
30	−8.23	Asp54 (2.87, 2.74) Asp140 (2.73) Asn 135 (2.97) Phe1 (2.92, 3.00) Asp47 (2.95) Gln133 (3.10)	Tyr48, Asp47, Ile13, Ile52, Glu50	Tyr48 (pi-pi) (3.67)
	−7.52	Asp54 (2.70, 2.70) Asp140 (2.74) Asn135 (2.92) Phe1 (2.96, 2.93) Asp47 (2.91) Gln133 (3.13)	Ile13, Asp140, Asp47, Phe142, Phe1, Ile52, Tyr48	———
31	−7.63	Asp54 (2.71, 2.74) Asp140 (2.81) Asn135 (2.88) Phe1 (2.82, 2.93) Asp47 (2.91) Gln133 (3.14)	Tyr137, Tyr48, Asp140, Phe1, Ile13, Ile52, Asp47	H_2O782 water bridge to Asp140 (3.16)

(*continued on next page*)

Table 2 (*continued*)

Compd.	Score kcal/mol	H-bond interactions (Å)	Hydrophobic interactions	Other interactions (Å)
32	−6.89	Asp54 (2.76, 2.90) Asn135 (2.90) Phe1 (2.94, 3.03) Asp47 (2.79) Asp140 (2.84)	Tyr48, Tyr137, Ile13, Ile52, Asp140, Phe1, Asp47	———

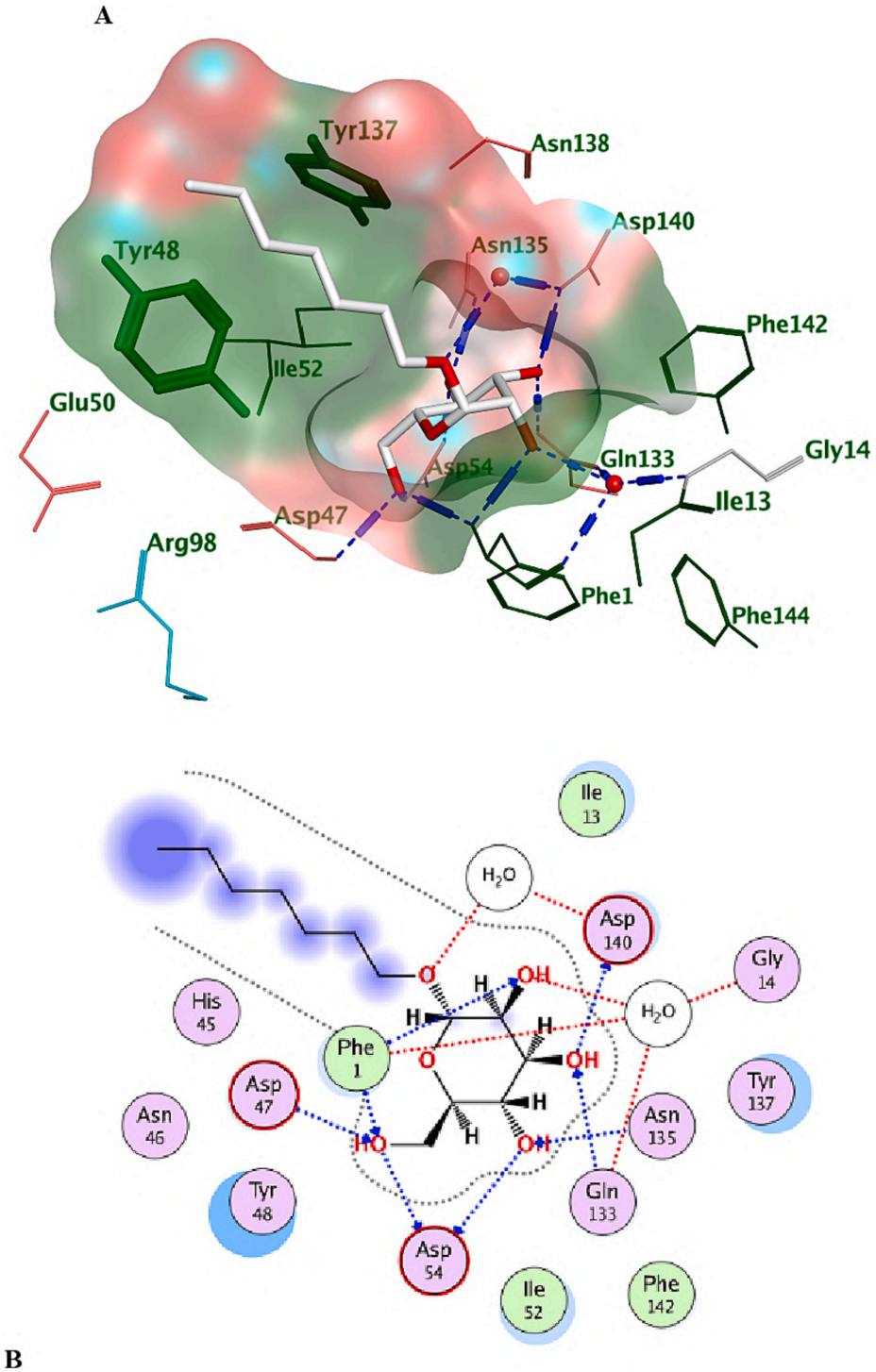

Fig. 2. 3D (A) and 2D (B) Ligplots of **HM** within the active site of FimH (PDB: 4XO8).

Table 3
Some molecular descriptors of aryl chains of compounds **24**–**32** compared with *n*-heptyl chain of **HM**.

Moiety	Compd No	THSA	TPSA	THSA/ TPSA
n-heptyl alcohol	HM	286.62	20.23	14.11
Phenyloxadiazole-2-thiol	**24**	218.00	77.72	2.80
4-Hydroxyphenyloxadiazole-2-thiol	**25**	186.93	97.95	1.91
4-Pyridyloxadiazol-2-ylthiol	**26**	194.20	90.61	2.14
3-Pyridyloxadiazole-2-thiol	**27**	192.27	90.61	2.12
4-Bromobenzyloxadiazole-2-thiol	**28**	280.08	77.72	3.60
4'-hydroxybiphen-4-ylmethyloxadiazole-2-thiol	**29**	323.47	97.95	3.30
Biphen-4-yloxymethyloxadiazole-2-thiol	**30**	374.74	86.95	4.31
Benzylthiol	**31**	249.81	38.80	6.43
Benzothiazol-2-ylthiol	**32**	237.63	51.69	4.60

As reported, there is a stacking interaction between Tyr48 and the second thiazole ring of NeoTazman [28]. In a previous study [59], local hardness; η(r) and polarizability (α) were reported as validated reactivity descriptors for ligand affinity in the tyrosine gate. These descriptors were calculated for compounds **31** and **32** that exhibited good α = 41.8 and 43.8, respectively, as well as low η (r) = 8.9 and 7.9 Kcal/mol, respectively. Furthermore, the compounds' binding affinities were proved to depend mostly on the ratio of hydrophobicity to polarity of their aryl aglycones. These aglycones should maintain important hydrophobic interactions outside the mannose-binding pocket, consequently, augment their overall binding and confirm their potency. Thus, two descriptors; total hydrophobic surface area (THSA) and topological polar surface area (TPSA) (Table 3) were calculated for the aryl moieties and results compared with **HM**. Ligand benzyl and benzothiazolyl moieties of compounds **(31)** and **(32)** respectively were shown to have higher hydrophobicity to polarity ratios than their oxadiazole counterparts (**24**–**30**). Also, the ligands' aglycones were properly aligned past the heptyl chain of **HM** and thiazolyl moiety of NeoTazMan forming ~~strong~~ key staggered π-stacking with Tyr48 and *T*-shaped one with Tyr137 within the tyrosine gate (Fig. 3). Forming strong key staggered π-stacking with Tyr48 and *T*-shaped one with Tyr137 within the tyrosine gate (Fig. 3). In addition to other hydrophobic interactions the ligands exhibited with Asp140, Phe1, Ile13, Ile52, Asp47 residues. This conclusion might explain the superior potency of compounds **(31)** and **(32)** over their oxadiazole analogues. Moreover, amongst oxadiazole derivatives, it was observed that **(28)**, **(29)** and **(30)** analogues displayed the highest THSA/TPSA ratios (3.36–4.31). However, compounds **(28)** and **(30)** were less potent than **(29)** and consequently this might indicate another factor that disturbs ligand affinity. The ability of the aglycone to form stacking with Tyr48 and orient properly within the tyrosine gate could affect largely the binding affinity of a mannoside. Therefore, aglycone of **(29)** with 4 -hydroxybiphen-4-ylmethyl was found to display good orientation within the hydrophobic gate. Ligand $C_6H_4CH_2$ moiety creates better sandwich with Tyr48, while *p*-HOC_6H_4 chain pointed towards solvent and was positioned near Glu50-Arg98 residues with potential pi-cation interaction with guanidine residue of Arg98 (Fig. 4, **A)**. On the other hand, aglycone of **30** was observed to show two possible opposite orientations within the binding site. (Fig. 4, **A)**. On the other hand, aglycone of **30** was observed to compete between two opposite orientations within the binding site. In one orientation, the ligand biphenyl chain stacked with Tyr48 in an analogous mode to compound **29** (Fig. 4, **B)**. In the other orientation, the ligand biphenyl moiety is lying in a location that loses stacking with Tyr48 and the aryl aglycone is being upturned to interact hydrophobically with Phe1, Ile13, and Phe142 at the hydrophobic support frame (Fig. 4, **C**). This might be attributed to the more flexibility of OCH_2 group linking oxadiazole to biphenyl chain in **(30)** relative to aglycone of **(29)**. Similarly, **(28)** probes the binding site where the 4-bromobenzyl moiety positioned towards Asp47 without proper stacking with Tyr48. Also, aryl aglycones of the less potent compounds; **(25)**, **(26)** and **(27)** with 4-hydroxyphenyl, 4-pyridyl and 3-pyridyl, respectively, revealed two orientations either stacking with Tyr48 or trying to interact electrostatically with Arg98-Glu50 owing to their enhanced polarity (Fig. 5). On the other hand, although 5-phenyloxadiazole derivative; **(24)** displayed proper orientation within the tyrosine gate, it did not exhibit good potency in the biological results. The lower THSA/TPSA of phenyloxadiazole moiety might be the reason behind its weak activity. For further validation of docking results, induced fit docking was performed and results were comparable with semiflexible one (figures for compounds **31** and **32** are included in S1and S2). Results of the docking simulations and molecular descriptors calculations attributed to explain the FimH inhibition effects of the compounds (**24**–**32)** relative to their binding affinity within the active site. SAR study concluded that the higher THSA/TPSA ratio of the aryl aglycone could affect largely the strength of π-stacking with Tyr48 and thus ligand binding affinity. Also, the latter effect should be combined with the ability of aglycone to maintain proper orientation within the tyrosine gate (Fig. 6).

4. Conclusion

New aryl and heteroaryl thiomannosides FimH antagonists were designed, synthesized and their binding activities were evaluated by cell based binding inhibition, ELLSA, and biofilm inhibition assays and compared to the reference compound **HM**. Compounds **31** and **32** with benzyl and benzothiazolyl, respectively, proved to be better inhibitors than the reference **HM**. Molecular docking study reasonably explained the obtained biological results. Altogether, the results suggest that introducing an aryl or heteroaryl aglycone of sufficient hydrophobicity and of proper orientation within the tyrosine binding site considerably enhance binding affinity. Thiomannosides described herein represent potent FimH antagonists and are attractive leads as therapeutics for the treatment of *E. coli* infections.

5. Experimental

5.1. Chemistry

5.1.1. General

Starting materials, reagents, and solvents were purchased from commercial sources unless otherwise noted. Dry Dichloromethane (DCM) and dry methanol were purchased and stored over activated molecular sieves 3 Å or 4 Å for at least one day. Molecular sieves 3 Å and 4 Å were activated at 200 °C for 1 h immediately before use. Reactions were monitored by TLC using glass plates coated with silica gel 60 F254 (Merck) and visualized by using UV light (254 nm) and/or by charring with a molybdate solution (a 0.02 M solution of ammonium cerium sulfate dihydrate and ammonium molybdate tetrahydrate in aqueous 10 % H_2SO_4). Flash column chromatography was carried out on silica gel 60 (63–200 μm, Merck). The (IR) spectra (KBr discs) were recorded on a thermoscientific nicolet IS10 FT IR spectrometer (thermo Fischer scientific) at Faculty of Science, Assiut University, Assiut, Egypt. ^{1}H NMR spectra of intermediates were recorded on a Varian EM-360 L NMR spectrometer (60 MHz, Varian) at Faculty of Pharmacy, Assiut University, Assiut, Egypt. ^{1}H, ^{13}C, spectra were scanned on Avance-III, High-performance FT-NMR spectrometer (Bruker. biospin international AG-Switzeraland) at Faculty of Science, Zagazig University, Egypt. Chemical shifts are expressed in δ-values (ppm) relative to TMS as an internal standard or residual solvent signals ($CDCl_3$ or DMSO-d_6) as appropriate. Spectral data was subsequently analyzed using MestReNova and TopSpin Softwares. For measurement of optical rotations, a Perkin–Elmer 341 polarimeter was used (10 cm cells, Na D-line: 589 nm) at room temperature at department of pharmaceutical organic chemistry, Faculty of pharmacy, Assiut University.

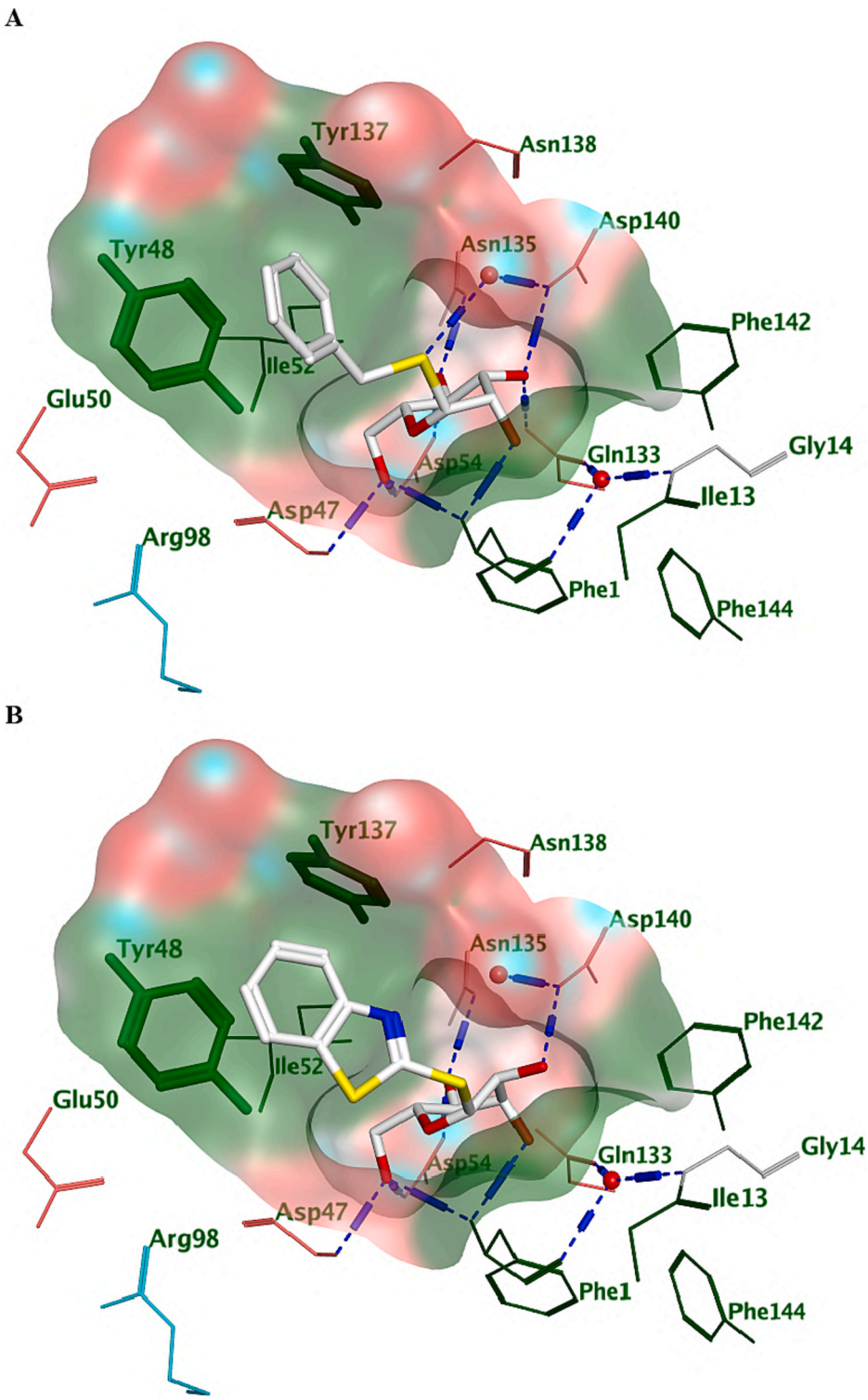

Fig. 3. 3D Ligplots of A; compound **31** and B; compound **32** within the active site of FimH (PDB: 4XO8).

5.1.2. Synthesis of 1,3,4-oxadiazole-2-thiols (8–14)

Carbon disulfide (0.11 g, 0.09 mL, 1.5 mmol) was slowly added to a solution of the appropriate acyl hydrazide (**1**–**7**) (0.5 mmol) and potassium hydroxide (0.03 g, 0.5 mmol) in EtOH (5 mL). The reaction mixture was refluxed for 5–6 h. Upon completion, the solvent was evaporated under reduced pressure and the residue was dissolved in water. The aqueous solution was acidified to pH 2 using conc HCl. The solid product was filtered and washed with water and dried. 5-Substituted-1,3,4-oxadiazole-2-thiols (**8**–**14**) were obtained with sufficient purity (70–85 % yield) to be used in further reactions without purification

5.1.2.1. 5-Phenyl-1,3,4-oxadiazole-2-thiol (8). mp 217–218 ℃ [49].

5.1.2.2. 4-(5-Mercapto-1,3,4-oxadiazol-2-yl)phenol (9). mp 227–228 °C [50].

5.1.2.3. 5-(Pyrid-4-yl)-1,3,4-oxadiazole-2-thiol (10). mp 269–270 ℃

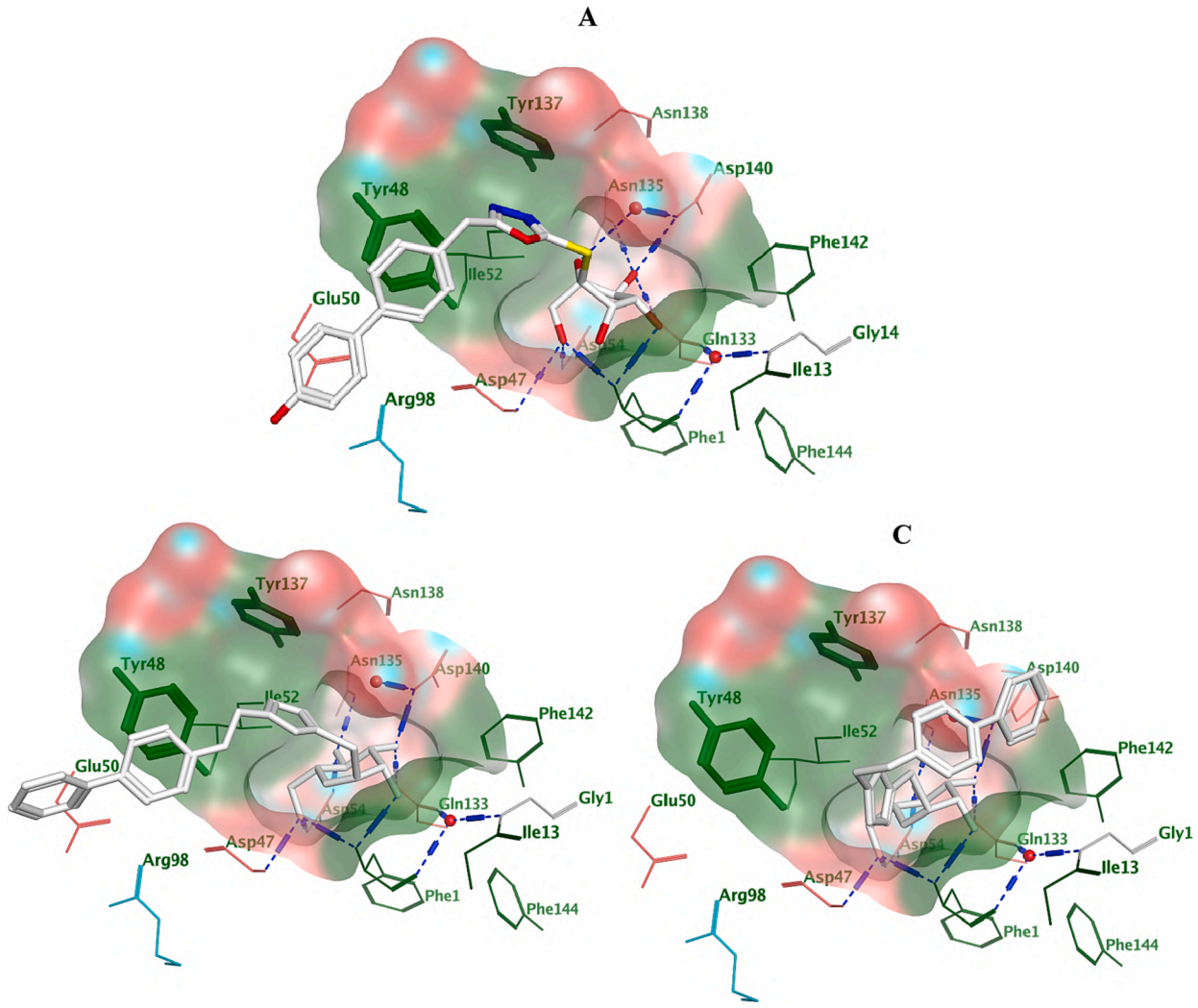

Fig. 4. 3D Ligplots of A; compound **29** and B; compound **30** with an orientation aligned past **29**, C; compound **30** with an orientation opposite to **29** within the active site of FimH (PDB: 4XO8).

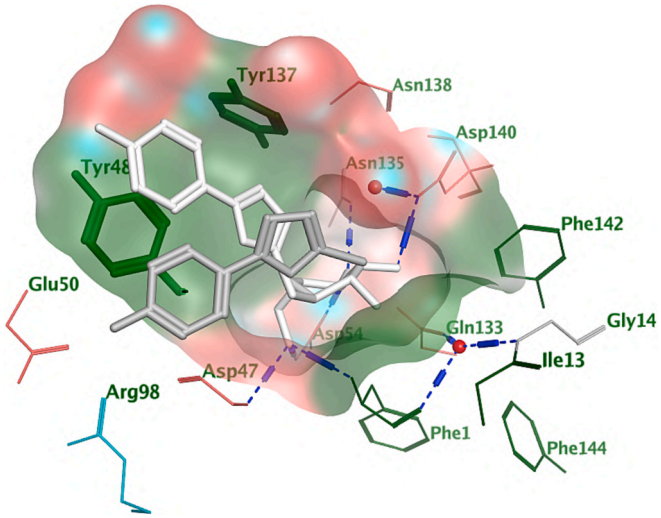

Fig. 5. Overlay 3D Ligplots of compound **25** within the active site of FimH (PDB: 4XO8) showing two possible orientations within tyrosine gate (white), outside tyrosine gate (grey).

[51].

5.1.2.4. 5-(3-Pyridyl)-1,3,4-oxadiazol-2-thiol (11). 232–233 ℃ [51].

5.1.2.5. 5-(4-Bromobenzyl)-1,3,4-oxadiazole-2-thiol (12). Yield: 85 %; mp 137–139 ℃; IR (KBr, ύ cm^{-1}): 3129, 3097, 2957, 2759, 1618, 1495, 1411, 1347, 1318, 1230, 1162, 1096, 958, 835, 819, 780, 691, 526; ^{1}H NMR (60 MHz, $CDCl_3$ + DMSO-d_6) δ = 7.50 (d, J = 9.0 Hz, 2H; ArH-3,5), 7.20 (d, J = 9.0 Hz, 2H; ArH-2,6), 4.03 (s, 2H; CH_2).

5.1.2.6. 4′-((5-Mercapto-1,3,4-oxadiazol-2-yl)methyl)-[1,1′-biphenyl]-4-ol (13). Yield: 70 %; mp 212–213 ℃; IR (KBr, ύ cm^{-1}): 3300, 3145, 2967, 2778, 1611, 1592, 1492, 1417, 1345, 1256, 1233, 1174, 1063, 974, 948, 833, 807, 649, 525; ^{1}H NMR (60 MHz, $CDCl_3$ + DMSO-d_6) δ = 7.65–7.23 (m, 7H; ArH), 7.13–7.07 (d, 2H, J = 9.0 Hz, ArH), 4.10 (s, 2H; CH_2).

5.1.2.7. 5-(([1,1′-Biphenyl]-4-yloxy)methyl)-1,3,4-oxadiazole-2-thiol (14). Yield: 77 %; mp 169–171 ℃; IR (KBr, ύ cm^{-1}): 3057, 3031, 2928, 2859, 2759, 1605, 1586, 1487, 1468, 1450, 1385, 1271, 1191, 949, 834, 768, 667, 529; ^{1}H NMR (60 MHz, $CDCl_3$ + DMSO-d_6) δ = 8.00–7.35 (m, 7H; ArH), 7.20 (d, 2H, J = 9.0 Hz, ArH), 5.30 (s, 2H; CH_2), 4.77 (brs, 1H; SH).

5.1.3. Synthesis of protected thio-α-D-mannopyranosides (15–23)

To a solution of D-mannose pentaacetate (0.5 g, 1.3 mmol) in dry

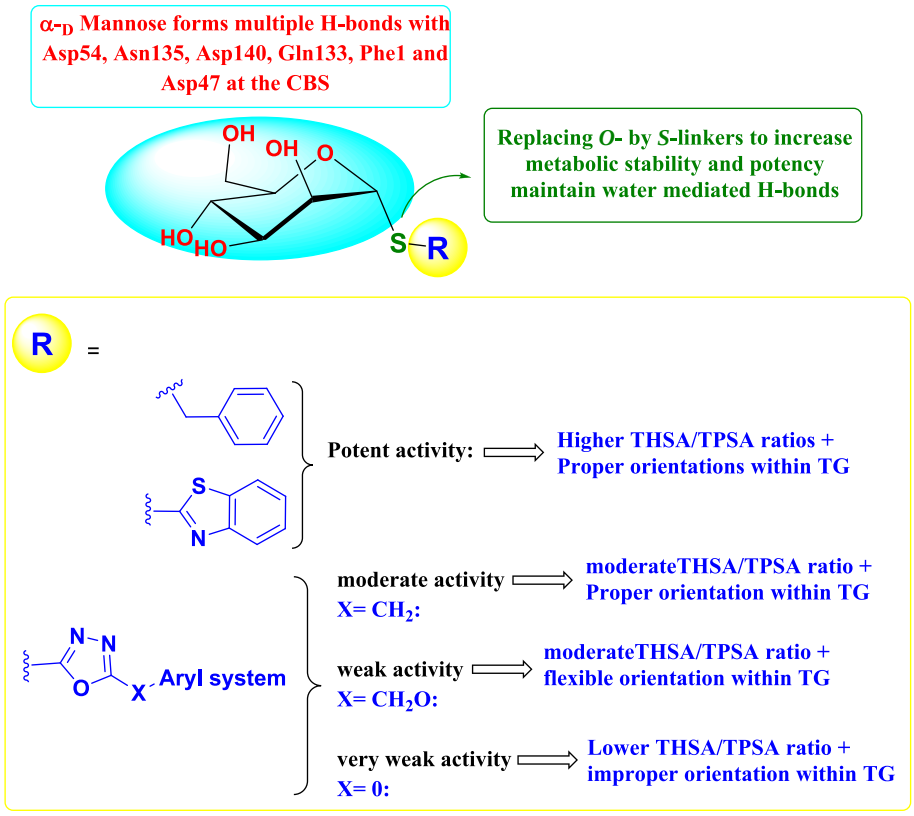

Fig. 6. Summary for SAR of the new thiomannosides.

DCM (10 mL), the appropriate thiol derivative (**8**–**14**) (1.6 mmol) was added. The reaction mixture was cooled to −10 °C with stirring, then BF_3-OEt_2 (0.5 mL, 5.5 mmol) was added dropwise slowly over 5 min. The reaction mixture was allowed to attain ambient temperature and stirred at this temperature for 24–48 h. Reaction mixture was quenched by addition of saturated Na_2CO_3 solution (5 mL). The organic layer was separated, and aqueous layer was extracted using DCM (10 mL x 3). The combined organic extracts were washed with brine (20 mL), dried over anhydrous Na_2SO_4, filtered and concentrated *in vacuo* to get the crude product. Compounds **22** and **23** were recrystallized from EtOAc/hexane to give 65 % and 70 % yields respectively. The crude products for compounds (**15**–**21**) were purified by column chromatography using EtOAc/hexane as gradient system (1/3 to 1/1). The desired α isomer was collected and concentrated to give (30–75 %) as colorless thick oil.

5.1.3.1. 2-((2,3,4,6-Tetra-O-acetyl-α-D-mannopyranos-1-yl)thio)-5-phenyl-1,3,4-oxadiazole (15). Reaction time 48 h; Yield: 75 %, ^{1}H NMR (60 MHz, $CDCl_3$) δ = 8.10 (d, J = 7.2 Hz, 2H, ArH), 7.80–7.43 (m, 3H, ArH), 6.30 (d, J = 3.6 Hz, 1H, H-1), 6.03, 6.17 (dd, J = 8.1, 3.1 Hz, 1H, H-3), 5.80 (t, J = 3.1 Hz, 1H, H-2), 5.65–5.20 (m, 1H, H-4), 4.70–3.90 (m, 3H, H-6, H-5, H-6′), 2.40–1.80 (m, 12H; $COCH_3$).

5.1.3.2. 2-((2,3,4,6-Tetra-O-acetyl-α-D-mannopyranos-1-yl)thio)-5-(4-hydroxyphenyl)-1,3,4-oxadiazole (16). Reaction time 48 h; Yield: 50 %; ^{1}H NMR (60 MHz, $CDCl_3$) δ = 7.85 (d, J = 8.1 Hz, 2H; ArH), 7.40 (s, 1H; OH), 7.00 (d, J = 8.1 Hz, 2H; ArH), 6.25 (d, J = 3.6 Hz, 1H; H-1), 6.07 (dd, J = 8.1, 3.1 Hz, H-3), 5.70 (t, J = 3.1 Hz, 1H, H-2), 5.60–5.25 (m, 1H, H-4), 4.50–4.10 (m, 3H, H-6, H-5, H-6′), 2.50–2.00 (m, 12H; $COCH_3$).

5.1.3.3. 2-((2,3,4,6-Tetra-O-acetyl-α-D-mannopyranos-1-yl)thio)-5-(pyrid-4-yl)-1,3,4-oxadiazole (17). Reaction time 48; Yield: 73 %; ^{1}H NMR (60 MHz, DMSO-d_6) δ = 8.85 (d, J = 6.0 Hz, 2H; ArH2,6), 7.86 (d, J = 6.1 Hz, 2H; ArH-3,5), 6.20 (d, J = 3.1 Hz, 1H; H-1), 5.97 (dd, J = 8.1, 3.1 Hz, 1H, H-3), 5.70 (t, J = 3.1 Hz, 1H, H-2), 5.35 (t, J = 6.3 Hz, 1H, H-4), 4.55–4.00 (m, 3H; H-6, H-5, H-6′), 2.40–2.00 (m, 12H; $COCH_3$).

5.1.3.4. 2-((2,3,4,6-Tetra-O-acetyl-α-D-mannopyranos-1-yl)thio)-5-(pyrid-3-yl)-1,3,4-oxadiazole (18). Reaction time 48 h; Yield: 70 %, ^{1}H NMR (60 MHz, $CDCl_3$) δ = 9.20 (s, 1H, ArH-2), 8.83 (br, 1H, ArH-6), 8.31 (d, J = 8.1, 1H; ArH-4), 7.70–7.50 (m, 1H; ArH-5), 6.20 (d, J = 3.1 Hz, 1H; H-1), 5.97 (dd, J = 8.1, 3.1 Hz, 1H, H-3), 5.70 (t, J = 3.1 Hz, 1H, H-2), 5.35 (d, J = 6.3 Hz, 1H, H-4), 4.55–4.00 (m, 3H, H-6, H-5, H-6′), 2.35–2.00 (m, 12H; $COCH_3$).

5.1.3.5. 2-((2,3,4,6-Tetra-O-acetyl-α-D-mannopyranos-1-yl)thio)-5-(4-Bromobenzyl)-1,3,4-oxadiazole (19). Reaction time 36 h; Yield: 70 %; ^{1}H NMR (60 MHz, $CDCl_3$) δ = 7.48 (d, J = 8.1 Hz, 2H, ArH-3,5), 7.17 (d, J = 8.1 Hz, 2H; ArH-2,6), 6.10 (d, J = 3.6 Hz, 1H, H-1), 5.78 (dd, J = 7.2, 3.1 Hz, 1H, H-3), 5.50 (t, J = 3.1 Hz, 1H, H-2), 5.43–5.10 (m, 1H, H-4), 4.20 (s, 2H; CH_2), 4.50–4.10 (m, 3H, H-6, H-5, H-6′), 2.40–1.80 (m, 12H; $COCH_3$).

5.1.3.6. 2-((2,3,4,6-Tetra-O-acetyl-α-D-mannopyranos-1-yl)thio)-5-((4′-hydroxy-[1,1′-biphenyl]-4-yl)methyl)-1,3,4-oxadiazole (20). Reaction tim e 48 h; Yield: 30 %; ^{1}H NMR (60 MHz, $CDCl_3$) δ = 7.80–7.30 (m, 6H), 7.00 (d, J = 8.1 Hz, 2H, ArH), 6.20 (d, J = 3.1 Hz, 1H; H-1), 6.83 (dd, J = 8.1, 3.1 Hz, 1H, H-3), 5.65 (t, J = 3.1 Hz, 1H, H-2), 5.50–5.20 (m, 1H, H-4), 4.50–4.10 (m, 5H, H-6, H-5, H-6′, CH_2), 2.50–2.00 (m, 12H; $COCH_3$).

5.1.3.7. 2-((2,3,4,6-Tetra-O-acetyl-α-D-mannopyranos-1-yl)thio)-5-(([1,1′-Biphenyl]-4-oxy)methyl)-1,3,4-oxadiazole (21). Reaction time 48 h; Yield: 65 %; ^{1}H NMR (60 MHz, $CDCl_3$) δ = 7.80 –7.25 (m, 7H, ArH), 7.10 (d, J = 8.8 Hz, 2H, ArH-2′,6′), 6.20 (d, J = 3.1 Hz, 1H;H-1), 6.37 (dd, J = 8.1, 3.1 Hz, 1H, H-3), 5.63 (t, J = 3.1 Hz, 1H, H-2), 5.33 (t, J =

6.3 Hz, 1H, H-4), 5.20 (s, 2H; CH_2), 4.50–4.00 (m, 3H, H-6, H-5, H-6′), 2.50–2.00 (m, 12H; $COCH_3$).

5.1.3.8. Benzylthio 2,3,4,6-tetra-O-acetyl-α-D-mannopyranoside (22). [52,53].

5.1.3.9. 2-((2,3,4,6-Tetra-O-acetyl-α-D-mannopyranos-1-yl)thio)benzo[d] thiazole (23). Reaction time 24 h; Yield: 75 %; ^{1}H NMR (60 MHz, $CDCl_3$) δ = 8.03–7.67 (m, 2H; ArH-4,7), 7.60–7.30 (m, 2H; ArH-5,6), 6.33 (s, 1H; H-1), 5.80–5.20 (m, 3H, H-2, H-3, H-4), 4.60–3.90 (m, 3H, H-6, H-5, H-6′), 2.40–2.00 (m, 12H; $COCH_3$).

5.1.3.10. n-Heptyl 2,3,4,6-tetra-O-acetyl-α-D-mannopyranoside. [19,52, 54].

5.1.4. Synthesis of the target thio-α-D-mannopyranosides (24–32)

To a solution of the protected compound **(15–23)** (0.2 g) in MeOH (5 mL), MeONa solution (25 % in MeOH) (2–3 drops) was added. The resulting reaction mixture was stirred at ambient temperature for 12–24 h. After completion of the reaction, the reaction mixture was acidified by addition of DOWEX-50 resin. to pH 3–4. After 10 min of stirring, the resin was removed by filtration, washed with MeOH (5 mL), the filtrate was evaporated under vacuum. The residue was washed with chloroform and recrystallized from MeOH.

5.1.4.1. 2-((α-D-Mannopyranos-1-yl)thio)-5-phenyl-1,3,4-oxadiazole (24). Reaction time 12 h; Yield: 75 % as a white solid; $[\alpha]_D^{25}$ + 88 (C 0.1, MeOH); ^{1}H NMR (400 MHz, DMSO-d_6) δ = 7.93 (d, J = 7.3 Hz, 2H; ArH-2,6), 7.68 (t, J = 7.2 Hz, 1H; ArH-4), 7.62 (t, J = 7.2 Hz, 2H; ArH-3,5), 5.97 (d, J = 5.7 Hz, 1H; H-1), 5.42–5.29 (m, 1H, H-3), 5.19–5.13 (m, 2H, H-2, H-4), 4.62 (t, J = 5.9 Hz, 1H, H-6), 4.29–4.16 (m, 1H, H-5), 4.02 (t, J = 4.1 Hz, 1H, H-6′), 3.78 (td, J = 6.5, 3.2 Hz, 1H, H-5), 3.70–3.59 (m, 2H, 2 OH), 3.58–3.51 (m, 1H, OH); ^{13}C NMR (100 MHz, DMSO-d_6) δ = 176.93, 158.43, 132.76, 129.57, 126.34, 121.98, 83.55, 79.05, 71.61, 68.56, 67.23, 60.94; Analysis calc. for $C_{14}H_{16}N_2O_6S$ (340.35): C, 49.41; H, 4.74; N, 8.23; S, 9.42. Found: C, 49.63; H, 4.85; N, 8.50; S, 9.47.

5.1.4.2. 5-(4-Hydroxyphenyl)-2-((α-D-mannopyranos-1-yl)thio)-1,3,4-oxadiazole (25). Reaction time 12 h; Yield: 70 % as a white solid; $[\alpha]_D^{25}$ + 56 (C 0.1, MeOH); ^{1}H NMR (400 MHz, DMSO-d_6) δ = 7.60 (d, J = 8.7 Hz, 2H; ArH-3,5), 6.70 (d, J = 8.7 Hz, 2H; ArH-2,6), 5.92 (d, J = 5.7 Hz, 1H; H-1), 5.75 (s, 1H; OH), 4.16 (dd, J = 5.7, 3.1 Hz, 1H, H-2), 4.02 (dd, J = 5.3, 3.2 Hz, 1H, H-3), 3.76 (td, J = 7.0, 3.3 Hz, 1H, H-4), 3.70–3.50 (m, 3H, H-6, H-5, H-6′); ^{13}C NMR (100 MHz, DMSO-d_6) δ 176.25, 159.61, 128.38, 128.33, 117.61, 83.40, 78.91, 71.66, 68.59, 67.34, 61.06; Analysis calc. for $C_{14}H_{16}N_2O_7S$ (356.35): C, 47.19; H, 4.53; N, 7.86; S, 9.00. Found: C, 47.40; H, 4.67; N, 7.08; S, 9.12.

5.1.4.3. 2-((α-D-Mannopyranos-1-yl)thio)-5-(pyrid-4-yl)-1,3,4-oxadiazole (26). Reaction time 16 h; Yield: 90 % as a white solid; $[\alpha]_D^{25}$ + 84 (C 0.1, MeOH); ^{1}H NMR (400 MHz, DMSO-d_6) δ = 8.85 (d, J = 6.0 Hz, 2H), 7.86 (d, J = 6.1 Hz, 2H, ArH), 5.98 (d, J = 5.8 Hz, 1H; H-1), 5.34 (d, J = 5.0 Hz, 1H; OH), 5.14 (d, J = 5.0 Hz, 1H; OH), 5.09 (d, J = 5.0 Hz, 1H; OH), 4.60 (t, J = 5.6 Hz, 1H; OH), 4.24–4.16 (m, 1H, H-2), 4.05–3.97 (m, 1H, H-3), 3.81–3.73 (m, 1H, H-4), 3.69–3.61 (m, 2H, H-6, H-5), 3.59–3.52 (m, 1H, H-6′); ^{13}C NMR (100 MHz, DMSO) δ = 177.15, 156.83, 151.06, 129.34, 119.83, 83.73, 79.10, 71.55, 68.48, 67.23, 60.85; Analysis calc. for $C_{13}H_{15}N_3O_6S$ (341.34): C, 45.74; H, 4.43; N, 12.31; S, 9.39. Found: C, 45.98; H, 4.59; N, 12.56; S, 9.52.

5.1.4.4. 2-((α-D-Mannopyranos-1-yl)thio)-5-(pyrid-3-yl)-1,3,4-oxadiazole (27). Reaction time 16 h; Yield: 90 % as a white solid; $[\alpha]_D^{25}$ + 67 (C 0.1, MeOH); ^{1}H NMR (400 MHz, DMSO-d_6) δ 9.09 (d, J = 2.3 Hz, 1H; ArH-2), 8.83 (dd, J = 4.9, 1.7 Hz, 1H; ArH-6), 8.31 (dd, J = 8.1, 2.0 Hz, 1H; ArH-4), 7.66 (dd, J = 8.1, 4.9 Hz, 1H; ArH-5), 5.98 (d, J = 5.7 Hz, 1H; H-1), 5.33 (d, J = 5.0 Hz, 1H; OH), 5.12 (d, J = 5.2 Hz, 1H; OH), 5.08 (d, J = 5.0 Hz, 1H; OH), 4.59 (t, J = 5.7 Hz, 1H; OH), 4.20 (dd, J = 5.4, 3.2 Hz, 1H, H-2), 4.02 (dd, J = 5.1, 3.1 Hz, 1H, H-3), 3.78 (td, J = 6.5, 3.3 Hz, 1H, H-4), 3.71–3.62 (m, 2H, H-6, H-5), 3.55 (dt, J = 11.9, 6.0 Hz, 1H; H-6′ H); ^{13}C NMR (100 MHz, DMSO-d_6) δ 177.41, 157.31, 153.49, 147.49, 134.55, 124.87, 119.33, 84.10, 79.52, 71.99, 68.94, 67.71, 61.32; Analysis calc. for $C_{13}H_{15}N_3O_6S$ (341.34): C, 45.74; H, 4.43; N, 12.31; S, 9.39. Found: C, 45.91; H, 4.60; N, 12.49; S, 9.61.

5.1.4.5. 5-(4-Bromobenzyl)-2-((α-D-mannopyranos-1-yl)thio)-1,3,4-oxadiazole (28). Reaction time 36 h; Yield: 85 % as a yellowish white solid; $[\alpha]_D^{25}$ + 60 (C 0.04, MeOH); ^{1}H NMR (400 MHz, DMSO-d_6) δ 7.58 (d, J = 8.0 Hz, 2H; ArH-3,5), 7.33 (d, J = 8.1 Hz, 2H; ArH-2,6), 5.84 (d, J = 6.2 Hz, 1H; H-1), 5.24 (d, J = 5.3 Hz, 1H; OH), 5.11 (d, J = 4.6 Hz, 1H; OH), 5.07 (d, J = 4.8 Hz, 1H; OH), 4.59 (t, J = 5.6 Hz, 1H; OH), 4.22 (s, 2H; CH_2), 4.09 (td, J = 5.7, 3.0 Hz, 1H, H-2), 3.89 (q, J = 4.3 Hz, 1H, H-3), 3.71–3.55 (m, 3H,H-4, H-6, H-5), 3.51 (dt, J = 11.6, 5.8 Hz, 1H, H-6′); ^{13}C NMR (100 MHz, DMSO-d_6) δ 177.41, 160.60, 132.56, 131.74, 131.46, 131.42, 120.84, 83.00, 71.66, 68.58, 66.84, 60.82, 30.32; Analysis calc. for $C_{15}H_{17}BrN_2O_6S$ (433.27): C, 41.58; H, 3.96; N, 6.47; S, 7.40. Found: C, 41.74; H, 4.17; N, 6.62; S, 7.49.

5.1.4.6. 5-((4′-Hydroxy-[1,1′-biphenyl]-4-yl)methyl)-2-((α-D-mannopyranos-1-yl)thio)-1,3,4-oxadiazole(29). Reaction time 48 h; Yield: 70 % as a yellowish white solid; $[\alpha]_D^{25}$ + 31 (C 0.045, MeOH); ^{1}H NMR (400 MHz, DMSO-d_6) δ = 8.50 (brs, 1H; OH), 7.59 – 7.54 (m, 2H; ArH-2′,6′), 7.50–7.47 (m, 2H; ArH-2,6), 7.38, 7.33 (two d, J = 7.7 Hz, 2H; ArH-3′,5′), 6.88–6.81 (m, 2H; ArH-3′,5′), 5.88, 5.85 (two d, J = 6.2 Hz, 1H; H-1), 5.33–5.29 (m, 1H, H-2), 5.19–5.11 (m, 2H, H-3, H-4), 4.66–4.59 (m, 1H, H-6), 4.20 (s, 2H; CH_2), 4.14–4.10 (m, 1H, H-5), 3.94–3.89 (m, 1H, H-6′), 3.71–3.55 (m, 3H, O—H), 3.56–3.52 (m, 1H, O—H); Analysis calc. for $C_{21}H_{22}N_2O_7S$ (446.47): C, 56.49; H, 4.97; N, 6.27; S, 7.18. Found: C, 56.71; H, 5.08; N, 6.45; S, 7.24.

5.1.4.7. 5-(([1,1′-Biphenyl]-4-oxy)methyl)-2-((α-D-mannopyranos-1-yl) thio)-1,3,4-oxadiazole (30). Reaction time 48 h; Yield: 80 % as a white solid; $[\alpha]_D^{25}$ + 56 (C 0.1, MeOH); ^{1}H NMR (400 MHz, DMSO-d_6) δ = 7.69 – 7.59 (m, 4H; ArH), 7.44 (td, J = 7.7, 1.9 Hz, 2H; ArH-3′,5′), 7.32 (td, J = 7.7, 1.7 Hz, 1H; ArH-4′), 7.16 (two d, J = 8.8 Hz, 2H; ArH-2′,6′), 5.90, 5.59 (2*d, J = 6.2 Hz, 1H; H-1), 5.38, 5.28 (two s, 2H; OCH_2), 5.31, 5.17 (two d, J = 5.2 Hz, 1H, H-2), 5.16, 5.09 (two d, J = 4.8 Hz, 1H, H-3), 5.11, 5.01 (two d, J = 4.6 Hz, 1H, H-4), 4.62 (t, J = 5.7 Hz, 1H), 4.14–3.87 (m, 2H, H-5, H-6), 3.53 (dd, J = 11.7, 5.8 Hz, 1H, H-6′); ^{13}C NMR (100 MHz, DMSO-d_6) δ = 177.46, 169.85, 157.79, 156.85, 156.79, 148.78, 139.59, 139.54, 134.05, 133.82, 128.91, 127.98, 127.95, 127.00, 126.96, 126.36, 126.32, 115.47, 115.38, 83.33, 80.65, 79.04, 78.90, 71.98, 71.71, 68.77, 68.58, 67.39, 66.97, 65.64, 60.88, 60.83, 59.80; Analysis calc. for $C_{21}H_{22}N_2O_7S$ (446.47): C, 56.49; H, 4.97; N, 6.27; S, 7.18. Found: C, 56.74; H, 5.13; N, 6.53; S, 7.30.

5.1.4.8. Benzylthio-α-D-mannopyranoside (31): $[\alpha]_D^{25}$ + 343. [52,53].

5.1.4.9. 2-((α-D-Mannopyranos-1-yl)thio)benzo[d]thiazole(32). Reaction time 24; Yield: 85 % as a white solid; $[\alpha]_D^{25}$ + 193 (C 1.51, MeOH); ^{1}H NMR (400 MHz, DMSO-d_6) δ = 8.01 (d, J = 7.8 Hz, 1H; ArH-4), 7.89 (d, J = 8.1 Hz, 1H; ArH-7), 7.48 (t, J = 7.8 Hz, 1H; ArH-6), 7.38 (t, J = 7.8 Hz, 1H; ArH-5), 6.18 (d, J = 4.8 Hz, 1H, H-1), 5.51–5.40 (m, 2H, H-2, H-3), 5.04–4.90 (m, 2H, H-4, H-6), 4.58 (br. s., 1H, H-5), 4.00 (br. s, 1H, H-6′); ^{13}C NMR (100 MHz, DMSO-d_6) δ 164.18, 152.37, 135.17, 126.54, 124.85, 121.87, 121.53, 88.05, 77.28, 71.76, 71.59, 66.63, 60.73; Analysis calc. for $C_{13}H_{15}NO_5S_2$ (329.04): C, 47.40; H, 4.59;; N, 4.25; S, 19.47. Found: C, 47.20; H, 4.63; N, 4.40; S, 19.60.

5.1.4.10. n-Heptyl α-D-mannopyranoside: $[\alpha]_D^{25}$ + 58 (C 1.0, MeOH). [19,54]

5.2. Biology

To investigate the new compounds interaction with FimH and *E. coli* and test their ability to inhibit adhesion and disrupt cell-bacteria interaction, the following experiments were done:

5.2.1. Effect of the new compounds (24–32) on the adhesion of E. coli to T24 urinary epithelial cells [55]

For adhesion assays, human urinary bladder epithelial cell line T24 (Nawah Scientific, Cairo, Egypt) was used. Cells were maintained in RPMI 1640 (Gibco, USA) supplemented with 10 % FBS (Gibco, USA) and incubated under an atmosphere containing 5 % CO_2 at 37 °C. Briefly, T24 urinary epithelial cells were seeded in 48-well tissue culture plates at a density of $1.5x10^5$ cells/well and incubated at 37 °C for 48 h. A preincubation protocol was used to test the ability of the drugs to prevent the attachment of *E coli* to host cells. *E. coli* strain isolated from patient with UTI was used as reference strain. Bacteria were grown overnight at 37 °C in Luria Bertani (LB) broth. The bacterial suspension for *in vitro* adhesion assays was prepared in sterile PBS. *E coli* was incubated for 1 h with compounds at the final concentration of 0.5 μM. Cells were then infected with the bacteria/drug mixture at a multiplicity of infection (MOI) of 10 for 3 h. Monolayers were washed three times with PBS and lysed with 1 % Triton X-100 (Sigma Aldrich, Germany) in deionized water. Samples were diluted and plated onto LB agar plates to determine the number of colony-forming units (CFUs). Levels of bacteria adhering to the cells in the presence of antagonists were expressed in percentages of residual bacteria, 100 % corresponding to adhesion in absence of any compound.

5.2.2. Competitive enzyme-linked lectinosorbent assay (ELLSA) [26,27]

RNase B (5 mg/mL) in carbonate/bicarbonate buffer (pH 9.6) was used to coat well of immunosorbent microplates. Plates were incubated at 4 °C overnight and then washed three times with PBS-containing Tween 20 (PBST, 0.15 %). To block the wells, bovine serum albumin (BSA, 3 %) in PBST was added, incubated for 2 h at 37 °C, then washed three times. Drugs (at a concentration of 0.5 μM) and FimH were added to wells, incubated for 1 h, then washed. Rabbit-anti-FimH IgG antibodies were added and incubated for 1 h, followed by a 1-hour incubation with goat anti-rabbit HRP-labeled secondary antibody (Enzo Life Sciences). For colorimetric detection, TMB was added, incubated in the dark for 15 min. The reaction was stopped with sulfuric acid and absorbance was read at 450 nm using a microplate reader (BioTek, USA).

5.2.3. Biofilm assay [56,57]

We further tested the ability of the compounds to inhibit bacterial adherence and biofilm formation by microtiter plate method. Compounds (0.5 μM) were seeded into 96-well microtiter plates, mixed with *E. coli* cultures, and incubated at 37 °C for 18 h. The cultures were removed, well were rinsed three times to remove unattached cells, and dried by heating at 56 °C for 1 h. Crystal violet aqueous solution (0.25 %) was added into the wells and left for 15 min, followed by rinsing the wells and dried overnight. Glacial acetic acid (200 μl) was added into the wells to dissolve the remaining crystal violet and the absorbance was measured at a wavelength of 570 nm, which corresponds to the mass of the biofilm in the well. All experiments were performed in triplicate, with mean and standard deviation calculated. These readings were then used to determine the percentage of biofilm inhibition as following:

$$PercentageofInhibition = [(OD_{Untreated} - OD_{Treated})/OD_{Untreated}] \times 100$$

5.2.4. Molecular docking

All the molecular modeling calculations and docking simulation studies were performed on a Processor Intel(R) Pentium(R) CPU N3510@ 1.99 GHz and 4 GB Memory with Microsoft Windows 8.1 pro (64 Bit) operating system using Molecular Operating Environment (MOE 2019.01, 2020; Chemical Computing Group, Canada) as the computational software. All MOE minimizations were performed until a RMSD gradient of 0.01 Kcal/mol/Å with the force field (MMFF94x) to calculate the partial charges automatically using Born solvation. Before simulations, the protein corrected, hydrogens are added and ionization states assigned, the system was optimized via protonation, and receptor was minimized using QuickPrep function. Water layer was retained during preparation and docking process. Triangle matching with London dG scoring was chosen for initial placement, and then the top 30 poses were refined using force field (MMFF94x) and GBVI/WSA dG scoring. The output database dock file was created with different poses for each ligand and arranged according to the final score function (S), which is the score of the last stage that was not set to zero.

CRediT authorship contribution statement

Anber F. Mohammed: Methodology, Writing – review & editing, Formal analysis. **Shimaa A. Othman:** Methodology, Investigation. **Ola F. Abou-Ghadir:** Writing – review & editing, Methodology. **Ahmed A. Kotb:** Methodology, Investigation. **Yaser A. Mostafa:** Supervision. **Mohamed A. El-Mokhtar:** Writing – original draft, Validation, Formal analysis, Data curation. **Hajjaj H.M. Abdu-Allah:** Conceptualization, Formal analysis, Funding acquisition, Investigation, Methodology, Project administration, Resources, Supervision, Validation, Writing – original draft, Writing – review & editing.

Declaration of competing interest

The authors declare that they have no known competing financial interests or personal relationships that could have appeared to influence the work reported in this paper.

Acknowledgement

The authors gratefully acknowledge financial support for competitional projects from Faculty of Pharmacy, Assiut University, Egypt.

Appendix A. Supplementary data

Supplementary data to this article can be found online at https://doi.org/10.1016/j.bioorg.2024.107258.

References

[1] D. Lebeaux, A. Chauhan, O. Rendueles, C. Beloin, From in vitro to in vivo models of bacterial biofilm-related infections, Pathogens. 2 (20135) 288-356.
[2] D. Lebeaux, J.M. Ghigo, C. Beloin, biofilm-related infections: bridging the gap between clinical management and fundamental aspects of recalcitrance toward antibiotics, Microbiol. Mol. Biol. Rev. 78 (2014) 510–543.
[3] O.F. Martínez, M.H. Cardoso, S.M. Ribeiro, O.L. Franco, Recent advances in anti-virulence therapeutic strategies with a focus on dismantling bacterial membrane microdomains, toxin neutralization, quorum-sensing interference and biofilm inhibition, Front. Cell. Infect. Microbiol. 9 (2019) 74.
[4] A. Asadi, S. Razavi, M. Talebi, M. Gholami, A review on anti-adhesion therapies of bacterial diseases, Infection 47 (2019) 13–23.
[5] J.P. Nataro, J.B. Kaper, Diarrheagenic *Escherichia coli*, Clin. Microbiol. Rev. 11 (1998) 142–201.
[6] L. Belanger, A. Garenaux, J. Harel, M. Boulianne, E. Nadeau, C.M. Dozois, *Escherichia coli* from animal reservoirs as a potential source of human extraintestinal pathogenic *E. coli*, FEMS Immunol. Med. Microbiol. 62 (2011) 1–10.
[7] S. Vanwetswinkel, A.N. Volkov, Y.G. Sterckx, A. Garcia-Pino, L. Buts, W. F. Vranken, J. Bouckaert, R. Roy, L. Wyns, N.A. van Nuland, Study of the structural and dynamic effects in the FimH adhesin upon α-D-heptyl mannose binding, J. Med. Chem. 57 (2014) 1416–1427.

[8] M.M. Sauer, R.P. Jakob, J. Eras, S. Baday, D. Eriş, G. Navarra, S. Bernèche, B. Ernst, T. Maier, R. Glockshuber, Catch-bond mechanism of the bacterial adhesion FimH, Nat. Commun. 7 (2016) 10738.

[9] M. Hartmann, T.K. Lindhorst, The bacterial lectin FimH, a target for drug discovery - carbohydrate inhibitors of type 1 fimbriae-mediated bacterial adhesion, Eur. J. Org. Chem. 3583–609 (2011).

[10] M. Totsika, M. Kostakioti, T.J. Hannan, M. Upton, S.A. Beatson, J.W. Janetka, S. J. Hultgren, M.A. Schembri, A FimH inhibitor prevents acute bladder infection and treats chronic cystitis caused by multidrug-resistant uropathogenic Escherichia coli ST13,1, J Infect Dis 208 (2013) 921–928.

[11] S. Cecioni, A. Imberty, S. Vidal, Glycomimetics versus multivalent glycoconjugates for the design of high affinity lectin ligands, Chem. Rev. 115 (2015) 525–561.

[12] L.K. Mydock-McGrane, T.J. Hannan, J.W. Janetka, Rational design strategies for FimH antagonists: new drugs on the horizon for urinary tract infection and crohn's disease, Expert Opin. Drug Discov. 12 (2017) 711–731.

[13] L. Mousavifar, R. Roy, Recent development in the design of small 'drug-like' and nanoscale glycomimetics against Escherichia coli infections, Drug Discov. Today 26 (2021) 2124–2137.

[14] N.E. Hatton, C. Baumann, M.A. Fascione, Developments in mannose-based treatments for uropathogenic Escherichia coli-induced urinary tract infections, Chembiochem 22 (2021) 613–629.

[15] L. Mousavifar, M. Sarshar, C. Bridot, D. Scribano, C. Ambrosi, A.T. Palamara, G. Vergoten, B. Roubinet, L. Landemarre, Julie bouckaert, rené Roy. insightful improvement in the design of potent uropathogenic *E. coli* FimH antagonists, Pharmaceutics 15 (2023) 527.

[16] S. Leusmann, P. Menova, E. Shanin, A. Titz, Christoph rademacher, glycomimetics for the inhibition and modulation of lectins, Chem. Soc. Rev. 52 (2023) 3663.

[17] C.S. Hung, J. Bouckaert, D. Hung, J. Pinkner, C. Widberg, A. DeFusco, C. G. Auguste, R. Strouse, S. Langermann, G. Waksman, S.J. Hultgren, Structural basis of tropism of *Escherichia coli* to the bladder during urinary tract infection, Mol. Microbiol. 44 (2002) 903–915.

[18] J. Bouckaert, J. Mackenzie, J.L. de Paz, B. Chipwaza, D. Choudhury, A. Zavialov, J. Karin Mannerstedt, D. Anderson, L.W. Piérard, P.H. Seeberger, S. Oscarson, H. De Greve, S.D. Knight, The affinity of the FimH fimbrial adhesin is receptor-driven and quasi-independent of Escherichia coli pathotypes, Mol. Microbiol. 61 (2006) 1556–1558.

[19] J. Bouckaert, J. Berglund, M. Schembri, E. De Genst, L. Cools, M. Wuhrer, C. S. Hung, J. Pinkner, R. Slattegård, A. Zavialov, D. Choudhury, S. Langermann, S. J. Hultgren, L. Wyns, P. Klemm, S. Oscarson, S.D. Knight, H. De Greve, Receptor binding studies disclose a novel class of high-affinity inhibitors of the Escherichia coli FimH adhesin, Mol. Microbiol. 55 (2005) 441–455.

[20] T. Klein, D. Abgottspon, M. Wittwer, S. Rabbani, J. Herold, X.H. Jiang, S. Kleeb, C. Lüthi, M. Scharenberg, J. Bezencon, E. Gubler, L.J. Pang, M. Smiesko, B. Cutting, O. Schwardt, B. Ernst, FimH antagonists for the oral treatment of urinary tract infections: from design and synthesis to in vitro and in vivo evaluation, J. Med. Chem. 53 (2010) 8627–8641.

[21] Z. Han, J.S. Pinkner, B. Ford, E. Chorell, J.M. Crowley, C.K. Cusumano, S. Campbell, J.P. Henderson, S.J. Hultgren, J.W. Janetka, Lead optimization studies on FimH antagonists: discovery of potent and orally bioavailable ortho-substituted biphenyl mannosides, J. Med. Chem. 55 (2012) 3945–3959.

[22] Z. Han, J.S. Pinkner, B. Ford, R. Obermann, W. Nolan, S.A. Wildman, D. Hobbs, T. Ellenberger, C.K. Cusumano, S.J. Hultgren, J.W. Janetka, Structure-based drug design and optimization of mannoside bacterial FimH antagonists, J. Med. Chem. 53 (2010) 4779–4792.

[23] L. Pang, S. Kleeb, K. Lemme, S. Rabbani, M. Scharenberg, A. Zalewski, F. Schadler, O. Schwardt, B. Ernst, FimH antagonists: structure-activity and structure-property relationships for biphenyl α-D-mannopyranosides, ChemMedChem 7 (2012) 1404–1422.

[24] W. Schonemann, J. Cramer, T. Mühlethaler, B. Fiege, M. Silbermann, S. Rabbani, P. D. Atwyler, P. Zihlmann, R.P. Jakob, C.P. Sager, M. Smieško, O. Schwardt, T. Maier, B. Ernst, Improvement of aglycone π-stacking yields nanomolar to sub-nanomolar FimH antagonists, ChemMedChem 4 (2019) 749–755.

[25] S. Kleeb, X. Jiang, P. Frei, A. Sigl, J. Bezençon, K. Bamberger, O. Schwardt, B. Erns, FimH antagonists: phosphate prodrugs improve oral bioavailability, J. Med. Chem. 59 (2016) 3163–3182.

[26] S. Brument, A. Sivignon, T.I. Dumych, N. Moreau, G. Roos, Y. Guérardel, T. Chalopin, D. Deniaud, R.O. Bilyy, A. Darfeuille-Michaud, J. Bouckaert, S. G. Gouin, Thiazolylaminomannosides as potent antiadhesives of type 1 piliated *Escherichia coli* isolated from crohn's disease patients, J. Med. Chem. 56 (2013) 5395–5406.

[27] T. Chalopin, D. Alvarez Dorta, A. Sivignon, M. Caudan, T.I. Dumych, R.O. Bilyy, D. Deniaud, N. Barnich, J. Bouckaert, S.G. Gouin, Second generation of thiazolylmannosides, FimH antagonists for E. coli-induced crohn's disease, Org. Biomol. Chem. 14 (2016) 3913–3925.

[28] D.A. Dorta, T. Chalopin, A. Sivignon, J. de Ruyck, T.I. Dumych, R.O. Bilyy, D. Deniaud, N. Barnich, J. Bouckaert, S.G. Gouin, Physiochemical tuning of potent *Escherichia coli* anti-adhesives by microencapsulation and methylene homologation, ChemMedChem 12 (2017) 986–998.

[29] X. Jiang, D. Abgottspon, S. Kleeb, S. Rabbani, M. Scharenberg, M. Wittwer, M. Haug, O. Schwardt, B. Ernst, Antiadhesion therapy for urinary tract infections—a balanced PK/PD profile proved to be key for success, J. Med. Chem. 55 (2012) 4700–4713.

[30] O. Schwardt, S. Rabbani, M. Hartmann, D. Abgottspon, M. Wittwer, S. Kleeb, A. Zalewski, M. Smiesko, B. Cutting, B. Ernst, Design, synthesis and biological evaluation of mannosyl triazoles as FimH antagonists bioorg, Med. Chem. 19 (2011) 6454–6473.

[31] L. Mydock-McGrane, Z. Cusumano, Z. Han, J. Binkley, M. Kostakioti, T. Hannan, J. S. Pinkner, R. Klein, V. Kalas, J. Crowley, N.P. Rath, S.J. Hultgren, J.W. Janetka, Antivirulence C-mannosides as antibiotic-sparing, oral therapeutics for urinary tract infections, J. Med. Chem. 59 (2016) 9390–9408.

[32] H. Al-Mughaid, Y. Jaradat, M. Khazaaleh, I. Al-Taani, Click chemistry inspired facile one-pot synthesis of mannosyl triazoles and their hemagglutination inhibitory properties: the effect of alkyl chain spacer length between the triazole and phthalimide moieties in the aglycone backbone, Carbohydr. Res. 534 (2023) 108965.

[33] Z. Car, T. Hrenar, V.P. Perokovic, R. Ribic, M. Senicar, S. Tomic, Mannosylated *N*-aryl substituted 3-hydroxypyridine-4-ones: synthesis, hemagglutination inhibitory properties, and molecular modeling, Chem. Biol. Drug Des. 84 (2014) 393–401.

[34] T. Tomasic, S. Rabbani, M. Gobec, I.M. Rascan, C. Podlipnik, B. Ernst, M. Anderluh, Branched α-D-mannopyranosides : a new class of potent FimH antagonists, MedChemComm. 5 (2014) 1247–1253.

[35] J. de Ruyck, M.F. Lensink, J. Bouckaert, Structures of C-mannosylated anti-adhesives bound to the type 1 fimbrial FimH adhesin, IUCrJ. 3 (2016) 163–167.

[36] J.A. Sattigeri, M. Garg, P. Bhateja, A. Soni, A.R.A. Rauf, M. Gupta, M.S. Deshmukh, T. Jain, N. Alekar, T.K. Barman, P. Jha, T. Chaira, R.B. Bambal, D.J. Upadhyay, T. Nishi, Synthesis and evaluation of thiomannosides, potent and orally active FimH inhibitors, Bioorg. Med. Chem. Lett. 28 (2018) 2993–2997.

[37] C. Jarvis, Z. Han, V. Kalas, R. Klein, J.S. Pinkner, B. Ford, J. Binkley, C. K. Cusumano, Z. Cusumano, L. Mydock-McGrane, S.J. Hultgren, J.W. Janetka, Antivirulence isoquinolone mannosides: optimization of the biaryl aglycone for FimH lectin binding affinity and efficacy in the treatment of chronic UTI, ChemMedChem 11 (2016) 367–373.

[38] M. Scharenberg, O. Schwardt, S. Rabbani, B. Ernst, Target selectivity of FimH antagonists, J. Med. Chem. 55 (2012) 9810–9816.

[39] L. Mousavifar, M. Touaibia, R. Roy, Development of mannopyranoside therapeutics against adherent-invasive *Escherichia coli* infections, Acc. Chem. Res. 51 (2018) 2937–2948.

[40] I. Yazgan, N.M. Noah, O. Toure, S. Zhang, O.A. Sadik, Biosensor for selective detection of *E. coli* in spinach using the strong affinity of derivatized mannose with fimbrial lectin, Biosens. Bioelectron. 61 (2014) 266–273.

[41] H.H.M. Abdu-Allah, S.-C. Wu, C.-H. Lin, Y.-Y. Tseng, Design, synthesis and molecular docking study of α-triazolylsialosides as non-hydrolyzable and potent CD22 ligands, Eur. J. Med. Chem. 208 (2020) 112707.

[42] R. Hevey, Strategies for the development of glycomimetic drug candidates, Pharmaceuticals 12 (2019) 55.

[43] (a) X. Liao, V. Vetvicka, D. Crich, Synthesis and evaluation of 1,5-dithia-D-laminaribiose, triose, and tetraose as truncated β-(1→3)-glucan mimetics, J. Org. Chem. 83 (2018) 14894–14904;
(b) B.R. Beno, K.-S. Yeung, M.D. Bartberger, L.D. Pennington, N.A. Meanwell, A survey of the role of noncovalent sulfur interactions in drug design, J. Med. Chem. 58 (2015) 4383–4438.

[44] H.H.M. Abdu-Allah, K. Watanabe, K. Hayashizaki, C. Takaku, T. Tamanaka, H. Takematsu, Y. Kozutsumi, T. Tsubata, H. Ishida, M. Kiso, Potent small molecule mouse CD22-inhibitors: exploring the interaction of the residue at C-2 of sialic acid scaffold, Bioorg. Med. Chem. Lett. 19 (2009) 5573–5575.

[45] D. Schwizer, H. Gäthje, S. Kelm, M. Porro, O. Schwardt, B. Ernst, Antagonists of the myelin-associated glycoprotein: a new class of tetrasaccharide mimics, Bioorg. Med. Chem. 14 (2006) 4944.

[46] J. Boström, A. Hogner, A. Llinàs, E. Wellner, A.T. Plowright, Oxadiazoles in medicinal chemistry, J. Med. Chem. 55 (2012) 1817–1830.

[47] T. Glomb, P. Świątek, Antimicrobial activity of 1,3,4-oxadiazole derivatives, Int. J. Mol. Sci. 22 (2021) 6979.

[48] C. Tresse, R. Radigue, R.G.V. Borowski, M. Thepaut, H.H. Le, F. Demay, S. Georgeault, A. Dhalluin, A. Trautwetter, G. Ermel, C. Blanco, P. van de Weghe, M. Jean, J.-C. Giard, R. Gillet, Synthesis and evaluation of 1,3,4-oxadiazole derivatives for development as broad-spectrum antibiotics, Bioorg. Med. Chem. 27 (2019) 115097.

[49] S. Joshi, A.V. Karnik, Facile conversion of acyldiithiocarbazinate salts to 1,3,4-oxadiazole derivatives under microwave irradiation, Synth. Commun. 32 (2002) 111–114.

[50] G. Karabanovich, J. Zemanová, T. Smutný, R. Székely, M. Šarkan, I. Centárová, A. Vocat, I. Pávková, P. Čonka, J. Němeček, J. Stolaříková, M. Vejsová, K. Vávrová, V. Klimešová, A. Hrabálek, P. Pávek, S.T. Cole, K. Mikušová, J. Roh, Development of 3,5-dinitrobenzylsulfanyl-1,3,4-oxadiazoles and thiadiazoles as selective antitubercular agents active against replicating and nonreplicating mycobacterium tuberculosis, J. Med. Chem. 59 (2016) 2362–2380.

[51] R. Ahmad, R. Iqbal, H. Akhtar, Synthesis and structure determination of some oxadiazole-2-thione and triazole-3-thione galactosides, Nucleosides Nucleotides Nucleic Acids 20 (2001) 1671–1682.

[52] M. Poláková, S. Šesták, E. Lattová, L. Petruš, J. Mucha, I. Tvaroška, J. Kóňa, α-D-mannose derivatives as models designed for selective inhibition of golgi α-mannosidase II, Eur. J. Med. Chem. 46 (2011) 944–952.
[53] M. Touaibia, E.-M. Krammer, T.C. Shiao, N. Yamakawa, Q. Wang, A. Glinschert, A. Papadopoulos, L. Mousavifar, E. Maes, S. Oscarson, G. Vergoten, M.F. Lensink, R. Roy, J. Bouckaert, Sites for dynamic protein-carbohydrate interactions of *O*- and *C*-linked mannosides on the *E. coli* FimH adhesin, Molecules 22 (2017) 1101.
[54] S. Andre, F.J. Cañada, T.C. Shiao, L. Largartera, T. Diercks, M. Bergeron-Briek, K. el Biari, A. Papadopoulos, J.P. Ribeiro, M. Touaibia, D. Solís, M. Menendez, J. Jimenez-Barbero, R. Roy, H.J. Gabius, Fluorinated carbohydrates as lectin ligands: biorelevant sensors with capacity to monitor anomer affinity in ^{19}F-NMR-based inhibitor screening, Eur. J. Org. Chem. 4364 (2012).
[55] M. Scharenberg, D. Abgottspon, E. Cicek, X. Jiang, O. Schwardt, S. Rabbani, B. Ernst, A flow cytometry- based assay for screening FimH antagonists, Assay Drug Dev. Technol. 9 (2011) 455–464.
[56] J.S. Pinkner, H. Remaut, F. Buelens, E. Miller, V. Aberg, N. Pemberton, M. Hedenström, A. Larsson, P. Seed, G. Waksman, S.J. Hultgren, F. Almqvist, Rationally designed small compounds inhibit pilus biogenesis in uropathogenic bacteria, PNAS 103 (2006) 17897–17902.
[57] M.G. Blango, M.A. Mulvey, Persistence of uropathogenic Escherichia coli in the face of multiple antibiotics, Antimicrob. Agents Chemother. 54 (2010) 1855–1863.
[58] Molecular Operating Environment (MOE), 2019.01 Chemical Computing Group ULC, 910-1010 Sherbrooke St. W., Montreal, QC H3A 2R7, Canada, 2020.
[59] G. Roos, A. Wellens, M. Touaibia, N. Yamakawa, P. Geerlings, R. Roy, L. Wyns, J. Bouckaert, Validation of reactivity descriptors to assess the aromatic stacking within the tyrosine gate of FimH, ACS Med. Chem. Lett. 4 (2013) 1085–1090.